STRUCTURAL BIOLOGY

Structures of dimeric human NPC1L1 provide insight into mechanisms for cholesterol absorption

Tao Long[1†], Yang Liu[1†], Yu Qin[1], Russell A. DeBose-Boyd[1], Xiaochun Li[1,2*]

Polytopic Niemann-Pick C1-like 1 (NPC1L1) plays a major role in intestinal absorption of biliary cholesterol, vitamin E (VE), and vitamin K (VK). The drug ezetimibe inhibits NPC1L1-mediated absorption of cholesterol, lowering of circulating levels of low-density lipoprotein cholesterol. Here, we report cryo–electron microscopy structures of human NPC1L1 (hNPC1L1) bound to either cholesterol or a lipid resembling VE. These findings, together with functional assays, reveal that the same intramolecular channel in hNPC1L1 mediates transport of VE and cholesterol. hNPC1L1 exists primarily as a homodimer; dimerization is mediated by aromatic residues within a region of transmembrane helix 2 that exhibits a horizonal orientation in the membrane. Mutation of tryptophan-347 lies in this region disrupts dimerization and the resultant monomeric NPC1L1 exhibits reduced efficiency of cholesterol uptake. These findings identify the oligomeric state of hNPC1L1 as a target for therapies that inhibit uptake of dietary cholesterol and reduce the incidence of cardiovascular disease.

INTRODUCTION

The absorption of dietary cholesterol involves solubilization by bile acids, transport across the apical membrane of enterocytes, and last, incorporation into chylomicrons that are secreted into the blood and lymph (*1*). Niemann-Pick C1-like 1 (NPC1L1) is a key mediator of extracellular cholesterol transport at the surface of the intestinal epithelium (*2*, *3*). To maintain intracellular homeostasis, cholesterol and natural sterols are secreted into bile by ABCG5/ABCG8 heterodimer (*4*, *5*) and NPC1L1 distributes on the apical membrane of hepatocytes to prevent excessive loss of biliary cholesterol (*6*). The prescription drug ezetimibe inhibits the transport activity of NPC1L1. The resultant decrease in intestinal cholesterol absorption triggers reactions in the liver that lead to the lowering of circulating levels of low-density lipoprotein (LDL) cholesterol, reducing the incidence of cardiovascular disease (*7*).

Previous studies showed that NPC1L1 mediates intestinal absorption of the nutrient coenzyme Q10 and the fat-soluble vitamins E (VE) and K (VK) (*8*–*10*). Considering that VE and VK are not synthesized by animals de novo, intestinal uptake of the vitamins is essential for maintenance of whole-body homeostasis. In addition to NPC1L1, scavenger receptor class B type I (SR-BI) and CD36 have been reported to mediate dietary uptake of VE and VK in the intestine (*11*–*13*). The mechanism through which VE and VK are transported across the membrane through NPC1L1, SR-BI, and CD36 remains unknown. Unlike cholesterol, a rigid and highly hydrophobic molecule, VE and VK have extremely flexible lipid tails and are considered to be more soluble than cholesterol.

The NPC1L1 protein is composed of 13 transmembrane domains (TMs), three extracellular domains, including an N-terminal domain (NTD), a middle extracellular domain (MLD), and a C-terminal domain (CTD), and a cytosolic tail that binds to Numb, a clathrin adaptor protein that triggers internalization of NPC1L1 (*14*). TMs 3 to 7 form a sterol-sensing domain (SSD) that is conserved in other membrane proteins involved in the metabolism and transport of cholesterol (NPC1, 3-hydroxy-3-methylglutaryl coenzyme A reductase, and sterol regulatory element-binding protein cleavage-activating protein) and cholesterol-mediated signaling (Patched1) (*15*–*17*). Structural analysis of Patched1 and NPC1 revealed that the SSD binds to a sterol molecule, which may serve as a gate to release the sterol into membranes (*18*–*21*).

NPC1L1 is structurally related to NPC1, which mediates export of LDL-derived cholesterol out of the lysosome. In 2009, a working model for NPC1-mediated transport of cholesterol from lysosomes was proposed (*22*). Following LDL receptor–mediated endocytosis, LDL is targeted to the lysosome where free cholesterol is liberated from the lipoprotein and delivered to a luminal protein called NPC2. Subsequently, NPC2 delivers cholesterol to the NTD of NPC1, which binds to the sterol (*23*). The NTD transfers bound cholesterol to the membrane domain of NPC1, which facilitates its translocation across the glycocalyx and lysosomal membrane. Several pieces of evidence indicate that NPC1 transports cholesterol through an intramolecular channel formed by the MLD, CTD, and SSD (*21*, *24*–*26*). NPC1L1 also contains an NTD that plays an essential role in cholesterol transport; however, delivery of dietary cholesterol to the NTD of NPC1L1 is mediated by the bile rather than a specific protein. The introduction of a point mutation (L216A) in the NTD of NPC1L1 abolishes the protein's ability to bind cholesterol and mediate its transport across the plasma membrane (*27*). Previous studies showed that NPC1L1 can traffic into the intracellular space through endocytosis (*28*–*30*). In contrast, NPC1 is sequestered in lysosomes to mediate transport of cholesterol across the lysosomal membrane en route to the endoplasmic reticulum (ER). The recent analysis of cryo–electron microscopy (cryo-EM) structures of rat NPC1L1 (rNPC1L1) revealed the presence of a cholesterol molecule embedded in an intramolecular channel within the protein's membrane domain. This channel is blocked by a derivative of ezetimibe, which helps to explain how the drug inhibits NPC1L1-mediated transport of cholesterol (*31*). It is well established that lipid profiles of rodents and humans differ substantially (*32*). Thus, the study of human NPC1L1 (hNPC1L1) merits further investigation that may provide insights into the dietary uptake of cholesterol.

[1]Department of Molecular Genetics, University of Texas Southwestern Medical Center, Dallas, TX 75390, USA. [2]Department of Biophysics, University of Texas Southwestern Medical Center, Dallas, TX 75390, USA.
*Corresponding author. Email: xiaochun.li@utsouthwestern.edu
†These authors contributed equally to this work.

RESULTS

Structures of hNPC1L1 with distinct lipid cargoes

We expressed full-length hNPC1L1 in the human embryonic kidney (HEK) 293S GnTI$^-$ cells. The protein is well behaved in detergent solution and deemed to be suitable for the structural determination by cryo-EM (fig. S1). The cryo-EM structure of hNPC1L1 was determined at 3.3-Å resolution (Fig. 1, A and B; Table 1; and fig. S2). The entire NTD can be observed in the low σ level (fig. S3A); however, the maps of NTD and TM1 are smashed after the postprocess, suggesting that the NTD adopts distinct conformations in the solution. Therefore, we did not build NTD and TM1 into the models. The C-terminal residues 1270 to 1285 form a helix that potentially interacts with a region of transmembrane helix 2, which exhibits a horizonal orientation in the membrane (designated pre-TM2) (Fig. 1C).

Notably, a lipid-like density more than 20 Å in length was found in the intramolecular channel of hNPC1L1 (Fig. 1D). The morphology of this density is much longer than cholesterol, implying a unique identity of this molecule. It has been shown previously that NPC1L1 can mediate transport of VE (*8*) and VK (*9*). The medium for protein expression contains 2% (v/v) fetal bovine serum including VE at a final concentration of ~0.3 mM. Thus, we tentatively modeled a VE molecule in the intramolecular channel, which revealed residues Trp^{383}, Met^{616}, Leu^{621}, Ile^{625}, Leu^{871}, Tyr^{886}, Phe^{887}, Leu^{890}, Ile^{1097}, and Phe^{1101} constitute a hydrophobic cavity that engages the lipid (Fig. 1D). VE, VK, derivatives, or metabolites of the vitamins may correspond to this density; however, the identification of this unknown lipid requires further investigation.

In contrast to other mammalian SSD-containing proteins [Patched1, Dispatched1, and NPC1 in the apo state (*20*, *26*, *33*–*37*)], our cryo-EM studies reveal that hNPC1L1 forms a dimer (Fig. 1A). Docking the NTD and TM1 into the dimeric structure of hNPC1L1 indicates that the NTD and TM1 are not involved in dimerization (fig. S3, A and B). Aromatic residues (Phe^{340}, Phe^{341}, Trp^{344}, Trp^{347}, and Trp^{351}) in the pre-TM2 form π-π interactions with the same aromatic residues in the other hNPC1L1 to trigger the dimerization (Fig. 1E and fig. S4A). Eukaryotic cholesterol transporters, such as NPC1, NPC1L1, and Patched1, have been shown to share high sequence homology with bacterial RND efflux pumps that can form oligomers (*38*, *39*) (fig. S4, B and C). Structural analysis suggests that the dimeric interface of hNPC1L1 is completely different from the resistance-nodulation-cell division transporters' oligomeric interface.

The previous work revealed that mouse Patched1 (PTCH1) was dimerized through its extracellular domains, which caused a unique bending of TMs (fig. S4D). Moreover, Sonic Hedgehog ligand can engage two Patched1 receptors yielding a signal competent complex, and the extracellular domains of PTCH1 might mediate the dimerization of the Hedgehog-PTCH1 complex (fig. S4, E and F). In these complexes, the TMs of PTCH1 molecules do not have direct contacts, indicating that the dimerization of NPC1L1 may occur through a distinct mechanism (fig. S4).

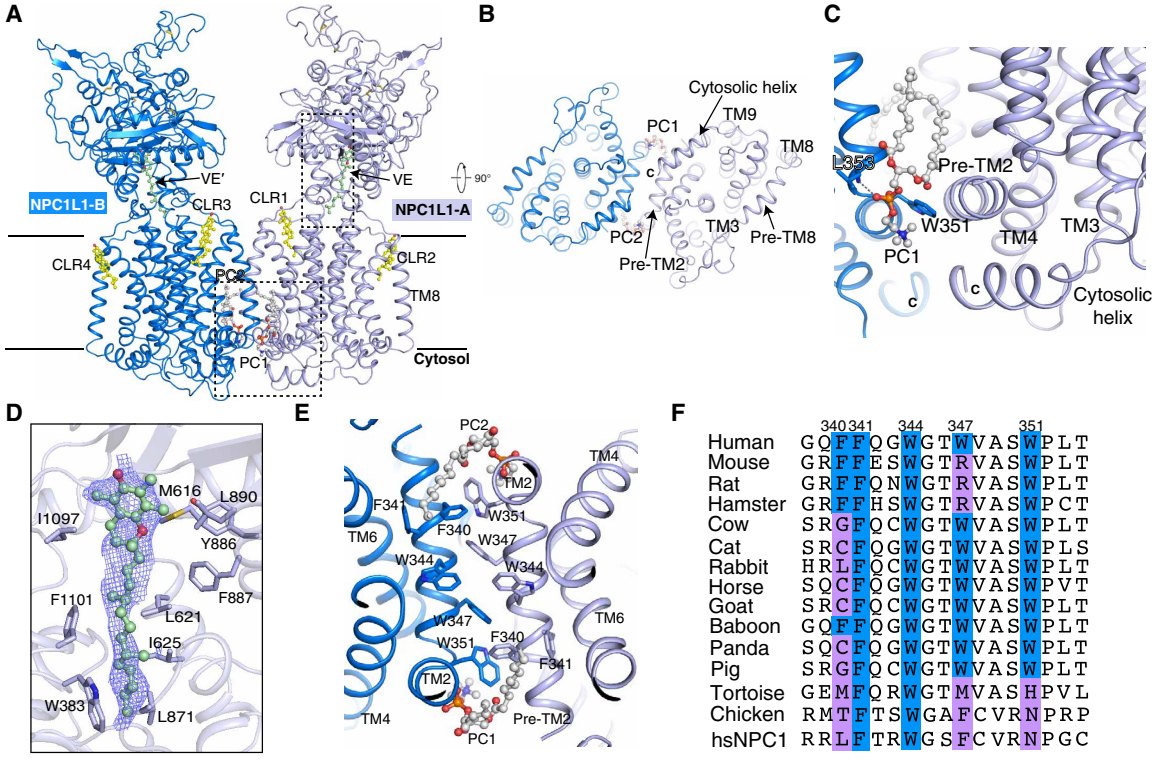

Fig. 1. Overall structure of VE-like lipid-bound hNPC1L1. (**A**) Overall structure of VE-like lipid–bound hNPC1L1 viewed from the side of the membrane. The cholesterols that bind to TMs of hNPC1L1 are shown in yellow sticks. The phospholipids (PC) are shown in gray sticks. The VE-like lipid molecules in the intramolecular channel are shown in green sticks. (**B**) The cytosolic view of TMs. (**C**) The interaction details between cytosolic helix and TMs. (**D**) The interaction details between VE-like lipid and hNPC1L1. The cryo-EM map of VE-like lipid is shown at 5σ level. (**E**) The interaction details of the dimeric interface. (**F**) The sequence alignment of pre-TM2 of NPC1L1 proteins (the species are indicated) and human NPC1 (hsNPC1). The conserved residues are highlighted.

Table 1. Cryo-EM data collection, refinement, and validation statistics.

	hNPC1L1-VE (EMDB: 24178) (PDB: 7N4U)	hNPC1L1-cholesterol (EMDB: 24179) (PDB: 7N4V)	$hNPC1L1_{W347R}$ (EMDB: 24180) (PDB: 7N4X)
Data collection and processing			
Magnification	60024	60024	60024
Voltage (kV)	300	300	300
Electron exposure (e–/Å^2)	60	60	60
Defocus range (μm)	−1.0 to −2.0	−1.0 to −2.0	−1.0 to −2.0
Pixel size (Å)	0.833	0.833	0.833
Symmetry imposed	C2	C2	C1
Initial particle images (no.)	779,251	1,001,780	1,421,700
Final particle images (no.)	135,911	251,678	186,790
Map resolution (Å)	3.34	3.58	3.33
FSC threshold, 0.143			
Refinement			
Initial model used (PDB code)	6V3H	hNPC1L1-VE	hNPC1L1-VE
Model resolution (Å)	3.50	3.64	3.35
FSC threshold, 0.5			
Map sharpening *B* factor (Å^2)	−114.9	−161.3	−117.8
Model composition			
Nonhydrogen atoms	15,396	15,390	7647
Protein residues	1906	1906	953
Ligands	8	8	3
B factors (Å^2)			
Protein	157.75	131.23	111.56
Ligand	155.95	123.61	111.00
R.M.S.D			
Bond lengths (Å)	0.014	0.014	0.014
Bond angles (°)	1.702	1.694	1.689
Validation			
MolProbity score	1.82	1.81	1.83
Clash score	4.81	6.06	5.53
Poor rotamers (%)	1.79	0.12	1.23
Ramachandran plot			
Favored (%)	94.53	92.22	92.53
Allowed (%)	5.26	7.78	7.47
Disallowed (%)	0.21	0.00	0.00

hNPC1L1 lacking the NTD shares a similar conformation with root mean square deviation (R.M.S.D.) of 1.9 Å for 904 residues of hNPC1, R.M.S.D. of 2 Å for 899 residues of rNPC1L1, and R.M.S.D. of 2.4 Å for 545 residues of hPatched1 (fig. S5, A to C). The position of the VE-like lipid tail in hNPC1L1 resembles the position of Hedgehog's palmitate in Patched1-Hedgehog complex (fig. S5C). However, VE-like lipid binds a higher position in hNPC1L1 than itraconazole in NPC1, which even extends into SSD (fig. S5B). The structure of rNPC1L1 bound to ezetimibe-PS (Eze-PS) showed that the inhibitor blocks the intramolecular channel of NPC1L1 to prevent lipid transport (fig. S5A). The structural comparison suggests that Eze-PS may also abolish NPC1L1-mediated transport of VE, which would be consistent with a previous study (*40*). Moreover, a cholesterol-like density found in the SSD at extracellular leaflet (CLR1 and CLR3 in Fig. 1A) is consistent with our previous findings in Patched1 (*18*, *33*) and Dispatched1 (*36*). As the working model of NPC1 and Patched1 (*17*), the SSD in hNPC1L1 may serve as an exit for cargoes that deliver lipid on the apical surface of enterocytes or hepatocytes.

We next purified hNPC1L1 in the presence of cholesterol during the entire procedure at a final concentration of 20 μM. The structure of cholesterol-bound hNPC1L1 was determined at 3.6-Å resolution (Fig. 2A, Table 1, and fig. S6). The VE-like lipid in the channel was replaced by a much shorter molecule corresponding to cholesterol (Fig. 2C). The position of cholesterol is deeper than VE-like lipid in the $hNPC1L1_{WT}$ and cholesterol in the rNPC1L1 but is similar to that in hNPC1 (Fig. 2B and D). Residue Gln^{873}, which is also conserved in the hNPC1, appears to interact with the 3-hydroxyl group of cholesterol (Fig. 2C). The structural comparison shows that the N terminus of TM5 in the SSD changes its conformation to engage the cholesterol in the binding pocket. Moreover, residue Val^{697} shifts 3 Å to provide sufficient room to accommodate the side chain of cholesterol (Fig. 2D).

VE and cholesterol absorbed via the channel of hNPC1L1

To validate the transport activity of hNPC1L1, we used a quantitative assay to measure the cholesterol uptake in rat liver CRL-1601 cells that stably express $hNPC1L1_{WT}$–Flag–GFP (green fluorescent protein) or $hNPC1L1_{L216A}$-Flag-GFP. Previous studies showed that CRL-1601 cells overexpressing NPC1L1 absorb cholesterol delivered by methyl-β-cyclodextrin (MCD) (*28*) or bile (*30*). In our assays, cells were first incubated with medium containing 1.5% (w/v) MCD for 30 min to deplete cellular cholesterol. This treatment condition ensured that the majority of NPC1L1 is localized on the cell surface at steady state (Fig. 3, A to C). Although dietary cholesterol and VE are solubilized in bile in the intestine and it has been reported that cyclodextrin treatment may block trafficking of membrane receptors (*30*), CRL-1601 cells do not tolerate incubation with bile over 30 min, which is required for us to use MCD for cholesterol delivery.

Cells were then treated with ^{3}H-cholesterol at a final concentration of 30 nM and various amounts of α-tocopherol (VE). After 30 min, cells were harvested, and both the GFP intensity and ^{3}H-cholesterol level were measured in the same lysates. This allowed us to normalize the cholesterol uptake by GFP intensity. The results show that cholesterol uptake through $hNPC1L1_{WT}$, but not $hNPC1L1_{L216A}$, was inhibited in the presence of α-tocopherol (Fig. 3D). The amount of cholesterol-MCD complex, which can be directly internalized into the cell, presents a basal absorption level (Fig. 3D). Notably, cholesterol uptake was not completely abolished by the addition to cells of

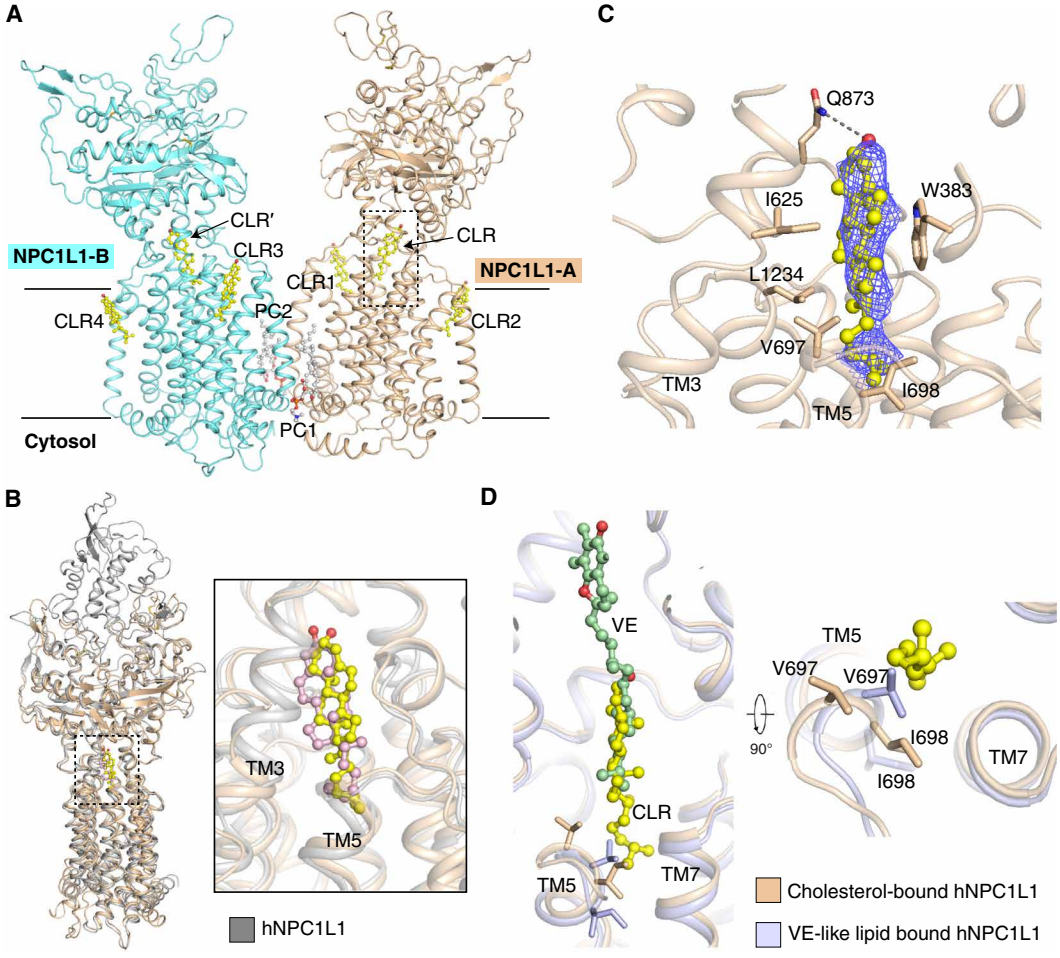

Fig. 2. Overall structure of cholesterol-bound hNPC1L1. (**A**) Overall structure of cholesterol-bound hNPC1L1 viewed from the side of the membrane. The cholesterols that bind to hNPC1L1 are shown in yellow sticks. The phospholipids (PC) are shown in gray sticks. (**B**) The structural comparison between cholesterol-bound hNPC1L1 and hNPC1 (PDB code: 6W5T). (**C**) The interaction details between cholesterol in the intramolecular channel and hNPC1L1. The cryo-EM map of cholesterol is shown at 5σ level. (**D**) The structural comparison of VE-like lipid and cholesterol in the intramolecular channel. The conformational changes in TM5 are shown. The residues that are involved in binding to cholesterol are shown in sticks.

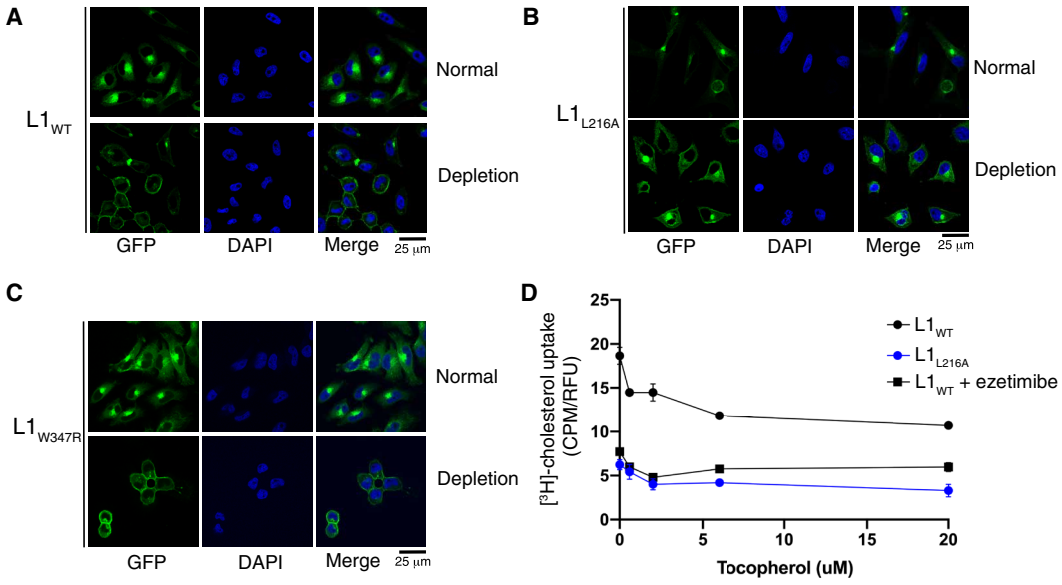

Fig. 3. Both α-tocopherol and cholesterol can be transported by the same intramolecular channel of hNPC1L1. (**A** to **C**) Localization of hNPC1L1 proteins in cells before and after depletion by 1.5% (w/v) MCD. The CRL-1601 cells stably expressing hNPC1L1$_{WT}$-Flag-GFP/hNPC1L1$_{L216A}$-Flag-GFP/hNPC1L1$_{W347R}$-Flag-GFP were fixed and stained with 4′,6-diamidino-2-phenylindole (DAPI; blue). Immunofluorescence microscopy was performed as described in Methods. Scale bars, 25 μm. (**D**) Competition assays. α-Tocopherol can complete with cholesterol in hNPC1L1$_{WT}$ (black circle)–mediated absorption. The hNPC1L1$_{L216A}$ (blue circle) serves as a negative control. hNPC1L1$_{WT}$ with ezetimibe (black square) was considered as background. CPM, counts per minute; RFU, relative fluorescence units. Data are means ± SD (n = 3).

excess α-tocopherol. We speculate that this disparity results from the mechanism through which lipid cargoes are delivered to cells. The previous findings also showed that NPC1L1-mediated uptake of VE and cholesterol can be inhibited by ezetimibe (*8*), which is also consistent with our data (Fig. 3D). Thus, we conclude that VE and cholesterol are transported through the same intramolecular channel of NPC1L1.

Physiological importance of hNPC1L1 dimer

Trp^{347} of hNPC1L1 is conserved in most mammalian species but not in rodents (Fig. 1F and fig. S5A). Previous structural analysis of rNPC1L1 revealed a monomeric state (*31*), which led us to posit that mutation of Try^{347} to arginine will disrupt the dimeric interface. The dimeric interface was disrupted by introducing Trp^{347}Arg mutation in the pre-TM2 (fig. S1). The structure of hNPC1L1$_{W347R}$ was determined at 3.3-Å resolution by cryo-EM (Fig. 4A, Table 1, and fig. S7). The overall structures of hNPC1L1$_{W347R}$ and hNPC1L1$_{WT}$ share a similar conformation with an R.M.S.D. of 0.6 Å. Notably, the density in the intramolecular channel is akin to a sterol-like molecule (Fig. 4A). Both the position of the endogenous ligand and the conformation of TM5 in hNPC1L1$_{W347R}$ are similar to the ligand and TM5 conformation in the cholesterol-bound dimeric hNPC1L1$_{WT}$ (fig. S8); therefore, a cholesterol has been modeled into the hNPC1L1$_{W347R}$ structure (Fig. 4A).

To validate the physiological significance of the dimer interface, we performed cholesterol uptake assays to evaluate transport activity of hNPC1L1$_{WT}$, hNPC1L1$_{W347R}$, and hNPC1L1$_{L216A}$. Cellular cholesterol was depleted by MCD for 30 min, and ^{3}H-cholesterol was then fed to cells at a final concentration of 20 nM for certain times. We measured GFP intensity of lysates and quantified internalized ^{3}H-cholesterol by scintillation counting; cholesterol uptake was normalized by GFP intensity (Fig. 4B). Both ezetimibe treatment and the loss-of-function mutation L216A can abolish the cholesterol uptake of hNPC1L1; therefore, ^{3}H-cholesterol uptake in these groups represents the background, which is caused by the internalized cholesterol-MCD complex. Thus, we took out the background by subtracting cholesterol uptake in ezetimibe-treated cells (triangles in Fig. 4B) from uptake data (circles in Fig. 4B). This quantitative analysis more clearly shows that the amount of cholesterol uptake via hNPC1L1$_{WT}$ is considerably higher than that via hNPC1L1$_{W347R}$ (Fig. 4C).

It was reported previously that ezetimibe-mediated inhibition of NPC1L1 triggers the proteolytic activation of the membrane-bound transcription factor SREBP-2 (*41*), which controls expression of genes encoding cholesterol biosynthetic enzyme and the LDL receptor (*42*). It is tempting to speculate that monomeric NPC1L1, which exhibits reduced activity in cholesterol absorption, cannot mediate cholesterol-dependent inhibition of SREBP-2. To appraise this hypothesis, we depleted cells of cholesterol by MCD and subsequently treated them with 37.5 μM cholesterol in fresh medium for 90 min. The cells were then further incubated in a lipoprotein-deficient medium for additional 120 min, allowing the cholesterol transferred from the endocytic recycling compartment to ER where the inhibition of SREBP cleavage occurs (*28*). The cells were harvested, lysed, and analyzed by immunoblot analysis using anti-rat SREBP-2 antibody. The results show that the nuclear forms of SREBP-2 in cells stably expressing hNPC1L1$_{WT}$/hNPC1L1$_{W347R}$/hNPC1L1$_{L216A}$ are similar following cholesterol depletion (Fig. 4D, lanes 1 to 3). Following treatment with cholesterol, the nuclear forms of SREBP-2 in hNPC1L1$_{WT}$-expressed cells decreased, indicating that accumulation of cholesterol in ER inhibits proteolytic activation. However, activation of SREBP-2 failed to be inhibited by cholesterol in cells expressing either hNPC1L1$_{W347R}$ or hNPC1L1$_{L216A}$ (Fig. 4D, lanes 4 to 6). This finding indicates that disruption of

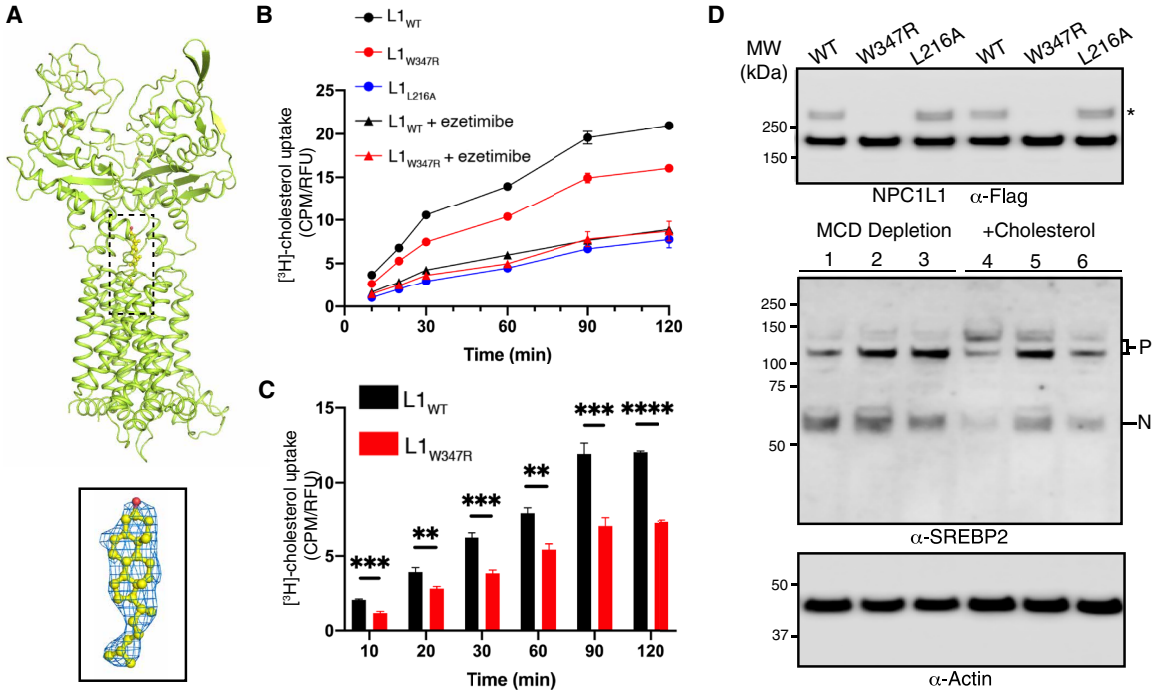

Fig. 4. The mutation W347R can disrupt the dimeric state of hNPC1L1 and attenuate the cholesterol uptake in cells. (**A**) The overall structure of hNPC1L1$_{W347R}$. Cryo-EM map of cholesterol in the intramolecular channel is shown at the 5σ level. (**B**) Uptake assays. After depletion, ^{3}H-cholesterol was supplemented into the medium at a final concentration of 20 nM. hNPC1L1$_{L216A}$ (blue circle) serves as a negative control. Data are means ± SD ($n = 3$). (**C**) The quantitative analysis of cholesterol uptake results of (B). Each column represents NPC1L1-specific cholesterol uptake amount. Cholesterol uptake in ezetimibe-treated cells was considered as background, and the amount was subtracted from the total uptake. The *P* value is calculated using *t* test. $^{**}P < 0.01$, $^{***}P < 0.001$, and $^{****}P < 0.0001$. (**D**) The SREBP-2 cleavage after depletion and replenishment of cholesterol. The expression levels of hNPC1L1 variants and actin are shown by Western blotting. The dimeric NPC1L1, precursor, and nuclear forms of SREBPs are denoted as *, P, and N, respectively.

dimeric hNPC1L1 not only interferes with cholesterol uptake but also prevents cholesterol-mediated inhibition of SREBP activation.

DISCUSSION

Dietary uptake is an indispensable source of sterols and fat-soluble vitamins in humans due, in part, to the unfavorable energetics of de novo synthesis of cholesterol and inability of human cells to produce VE and VK. NPC1L1 serves as an initial transporter in the intestine to mediate the uptake of cholesterol, plant sterols, VE, and VK from the diet. NPC1L1 is also expressed in hepatocytes where it helps to avoid excessive loss of biliary cholesterol by opposing ABCG5/ABCG8-mediated export of cholesterol. It is worthy of studying whether the liver NPC1L1 will transport the other biliary lipids into the hepatocytes.

Our current work suggests that these lipid cargoes share a similar transport mechanism across the intestinal epithelium via NPC1L1 (fig. S9). Our functional assays showed that the dimeric hNPC1L1 can mediate faster cholesterol uptake than its monomeric variant. Modulating the dimerization state of hNPC1L1 may attenuate cholesterol absorption in the intestine, which will maintain activation of SREBP-2 in the liver to enhance expression of LDL receptor that removes LDL cholesterol from the blood. Notably, the down-regulation of NPC1L1 by either small molecule (*7*, *43*) or protein (*44*) has been shown to lower the level of blood LDL cholesterol. The current study reveals the dimeric state of hNPC1L1 as a modality for development of therapies to prevent heart attack and stroke by lowering blood LDL cholesterol.

MATERIALS AND METHODS

Protein expression and purification

The cDNA of hNPC1L1 (gene ID: 29881) was cloned into pEG BacMam with a C-terminal Flag tag. The signal peptide of rNPC1L1 was used for replacing the native signal peptide of hNPC1L1 for promoting the protein expression. Point mutations were introduced into the coding region of NPC1L1 by site-directed mutagenesis using the QuikChange II XL Site-Directed Mutagenesis Kit (Agilent Technologies, Santa Clara, CA). The coding region of each plasmid was sequenced to ensure integrity of the construct. All the proteins were expressed using baculovirus-mediated transduction of mammalian HEK293S GnTI^{-} cells [American Type Culture Collection (ATCC)]. At 48 hours after infection, the cells were disrupted by sonication in buffer A, containing 20 mM Hepes (pH 7.5), 150 mM NaCl with 1 mM phenylmethylsulfonyl fluoride, and leupeptin (5 μg/ml). For cholesterol-bound wild-type hNPC1L1 protein, 20 μM cholesterol (solubilized in ethanol) was added in all purification steps. After low-speed centrifugation, the resulting supernatant was incubated in buffer A with 1% (w/v) lauryl maltose neopentyl glycol (Anatrace) for 1 hour at 4°C. The lysate was centrifuged again, and the supernatant was loaded onto a Flag-M2 affinity column (Sigma-Aldrich). After washing twice, the protein was eluted in buffer A with 0.06% (w/v) digitonin (Acros Organics) and 3× Flag peptide (100 μg/ml) and concentrated. The concentrated protein was purified by Superose 6 Increase size exclusion chromatography column (GE Healthcare) in a buffer containing buffer A and 0.06% (w/v) digitonin. The peak fractions were concentrated to 10 mg/ml for cryo-EM study.

EM sample preparation and imaging

The sample was added to Quantifoil R1.2/1.3 400 mesh Au holey carbon grids (Quantifoil), blotted using a Vitrobot Mark IV (FEI), and frozen in liquid ethane. The grids were imaged in a 300-keV Titan Krios (Field Electron and Ion Company, FEI) with a Gatan K3 Summit direct electron detector (Gatan). Data were collected at 0.833 Å/pixel with a dose rate of 23 electrons per physical pixel per second. Images were recorded for 1.8-s exposures in 60 subframes to give a total dose of 60 electrons/$Å^2$.

Imaging processing and 3D reconstruction

For VE-like lipid–bound hNPC1L1, 4736 images were collected. Dark subtracted images were first normalized by gain reference that resulted in a pixel size of 0.833 Å/pixel. Drift correction was performed using the program MotionCor2 (*45*). The contrast transfer function (CTF) was estimated using CTFFIND4 (*46*). To generate hNPC1L1 templates for automatic picking, around 3000 particles were manually picked and classified by two-dimensional (2D) classification in RELION-3 (*47*). After autopicking, the low-quality images and false-positive particles were removed manually. About 660,000 particles were extracted. The particles were 2D classified and 3D classified resulting in 282,917 good particles. After 3D autorefinement without a mask in RELION-3, a 4.54-Å map was obtained. The particles were re-extracted with a large box and then subjected to cryoSPARC (*48*). After 2D classification, heterogeneous refinement, and NU-Refinement in cryoSPARC, a final cryo-EM map of 3.34 Å was yielded using 135,911 good particles.

For cholesterol-bound hNPC1L1, 5904 images were collected. Dark subtracted images were first normalized by gain reference that resulted in a pixel size of 0.833 Å/pixel. Drift correction was performed using the program MotionCor2 (*45*). The CTF was estimated using CTFFIND4 (*46*). After autopicking, the low-quality images and false-positive particles were removed manually. About 1 million particles were extracted. The particles were subjected to cryoSPARC. After 2D classification, heterogeneous refinement, and NU-Refinement in cryoSPARC, a final cryo-EM map of 3.58 Å was yielded using 251,678 good particles.

For $hNPC1L1_{W347R}$, 5335 images were collected. Dark subtracted images were first normalized by gain reference that resulted in a pixel size of 0.833 Å/pixel. Drift correction was performed using the program MotionCor2 (*45*). The CTF was estimated using CTFFIND4 (*46*). After autopicking, the low-quality images and false-positive particles were removed manually. About 1.4 million particles were extracted. The particles were 2D classified and 3D classified resulting in 669,858 good particles. After 3D autorefinement without a mask in RELION-3, a 6.85-Å map was obtained. Bayesian polishing of particles were then performed using RELION-3. The 3D refinement using a soft mask and solvent-flattened Fourier shell correlations (FSCs) yielded a reconstruction at 4.14 Å. Then, a 3D classification without image alignment was performed. The best class containing 186,790 particles were refined using a soft mask, and solvent-flattened FSCs yielded a reconstruction at 3.81 Å. CTF refinement was performed, and the resulting particles were refined using a soft mask and solvent-flattened FSCs yielded a reconstruction at 3.33 Å. Applying a soft mask in RELION-3 postprocessing yielded a final cryo-EM map of 3.33 Å.

Model construction

For VE-like lipid–bound hNPC1L1 structure, the structure of rNPC1L1 with Eze-PS [Protein Data Bank (PDB) code: 6V3H] was docked to the map and then manually adjusted and refined using COOT (*49*). For cholesterol-bound hNPC1L1 and $hNPC1L1_{W347R}$ structures, the models were manually adjusted and refined using COOT based on the structure of VE-like lipid bound hNPC1L1. The densities of residues 22 to 332 and 1286 to 1332 were not resolved nor built.

Model refinement and validation

The models were refined in real space using PHENIX (*50*) and also in reciprocal space using Refmac with secondary structure restraints and stereochemical restraints (*51*). For cross-validations, the final model versus map FSC curve was generated in the comprehensive validation module in PHENIX. PHENIX and MolProbity (*52*) were used to validate the final model. Local resolutions were estimated using Resmap (*53*). Structure figures were generated using PyMOL (http://pymol.org) and Chimera (*54*).

Cell culture and establishment of stable cell lines

CRL-1601 cells were grown in monolayer at 37°C in 5% CO_2. The cells were maintained in medium A [Dulbecco's modified Eagle's medium containing penicillin (100 U/ml) and streptomycin sulfate (100 mg/ml)] supplemented with 10% fetal calf serum (FCS; Gibco, Thermo Fisher Scientific). Medium B was medium A supplemented with B-27 Supplement Minus AO (Gibco, Thermo Fisher Scientific), 10 μM compactin, and 50 μM mevalonate. Cholesterol-depleting medium was prepared by dissolving 1.5% (w/v) MCD (CTD Inc., Alachua, FL) into medium B. Different combinations of α-tocopherol, ^{3}H-cholesterol, and MCD were dried under N_2 and then resuspended in medium B to prepare various cholesterol-replenishing medium. The cDNAs of hNPC1L1, $hNPC1L1_{W347R}$, and $hNPC1L1_{L261A}$ (with native signal peptide) were cloned into pEGFP-N1 vector plasmid. These plasmids were transfected into CRL-1601 (McArdle RH7777, ATCC) cells with TransIT-2020 (Mirus Bio, Madison, MI) according to the user's manual. Then, CRL-1601 cells were selected by culturing in the presence of G418 sulfate (800 μg/ml; Gibco, Thermo Fisher Scientific). The cells were further subcloned to achieve monoclonality for the experiments.

Fluorescence microscopy

CRL-1601 cells that stably expressed $hNPC1L1_{WT}$-Flag-GFP/$hNPC1L1_{W347R}$-Flag-GFP/$hNPC1L1_{L216A}$-Flag-GFP were maintained in medium A with 10% FCS. For depleting, at 24 hours after seeding, the cells were treated with cholesterol depleting medium for 30 min at 37°C. Both depleted and untreated cells were fixed in 4% paraformaldehyde for 10 min at room temperature. The cells were washed with phosphate-buffered saline (PBS) and stained with 4′,6-diamidino-2-phenylindole (DAPI; 0.1 μg/ml) in the dark for 5 min at room temperature. The coverslips were then washed with PBS and mounted in Shandon Immu-mount (Thermo Fisher Scientific). Fluorescence images were acquired using a Plan-Apochromat ×63/1.4 oil differential interference contrast objective (Zeiss, Oberkochen, Germany), a Zeiss LSM 800 microscope (Zeiss), and ZEN imaging software (Zeiss).

Cholesterol uptake assay

Cholesterol-replenishing medium was prepared as follows. ^{3}H-cholesterol (American Radiolabeled Chemicals) and MCD were mixed and combined in a glass vial, and solvents were evaporated under N_2. The dried lipids were incorporated into medium B to a final concentration of 20 nM ^{3}H-cholesterol and 375 μM MCD. For

cholesterol uptake assay, on day 0, CRL-1601 cells that stably expressed hNPC1L1$_{WT}$-Flag-GFP/hNPC1L1$_{W347R}$-Flag-GFP/hNPC1L1$_{L216A}$-Flag-GFP were maintained in medium A with 10% FCS at a density of 6×10^4 cells per well of 24-well plates. On day 1, the cells were treated with cholesterol-depleting medium with 0.1% dimethyl sulfoxide (DMSO; control) or 50 μM ezetimibe (Sigma-Aldrich) for 30 min at 37°C. The cells were then switched to cholesterol-replenishing medium with 0.1% DMSO (control) or 50 μM ezetimibe. The cells were washed three times with 0.25% (v/v) bovine serum albumin (Sigma-Aldrich)–added PBS and lysed in buffer B [20 mM Hepes (pH 8.0), 150 mM NaCl, and 1% n-dodecyl-β-D-maltopyranoside). The GFP intensity of lysates was measured using an Epoch plate reader (BioTek) at a wavelength of 488 nm. The cholesterol uptake of the same lysates was then measured by scintillation counter (PerkinElmer). The cholesterol uptake was normalized by GFP intensity.

α-Tocopherol (VE) competition assay

VE competition medium was prepared as follows. ^{3}H-cholesterol, α-tocopherol (Sigma-Aldrich), and MCD were mixed and combined in a glass vial, and solvents were evaporated under N_2. The dried lipids were incorporated into medium B to a final concentration of 30 nM ^{3}H-cholesterol, 375 μM MCD, and various α-tocopherol. For competition assay, on day 0, CRL-1601 cells that stably expressed hNPC1L1 were grown in medium A with 10% FCS at a density of 6×10^4 cells per well of 24-well plates. On day 1, the cells were treated with cholesterol-depleting medium with 0.1% DMSO (control) or 50 μM ezetimibe for 30 min at 37°C. Then, the cells were switched to VE competition medium with 0.1% DMSO (control) or 50 μM ezetimibe. The cells were washed three times with PBS and lysed in buffer B. The GFP intensity of lysates was measured using an Epoch plate reader (BioTek, Winooski, VT) at a wavelength of 488 nm. The ^{3}H-cholesterol of the same lysates was measured by scintillation counter (PerkinElmer). The ^{3}H-cholesterol uptake was then normalized with relative GFP fluorescence.

SREBP-2 cleavage assay

On day 0, CRL-1601 cells that stably expressed hNPC1L1$_{WT}$-Flag-GFP/hNPC1L1$_{W347R}$-Flag-GFP/hNPC1L1$_{L216A}$-Flag-GFP were maintained in medium A with 10% FCS at a density of 2.5×10^5 cells per well of six-well plates. On day 1, the cells were treated with cholesterol-depleting medium for 30 min at 37°C. For detecting the SRBEP-2 cleavage after depleting cholesterol, the medium was removed, and then the cells were washed with PBS and switched to medium B for 2 hours at 37°C. For detecting the SRBEP-2 cleavage after refeeding cholesterol, the medium was removed, and then the cells were washed with PBS and switched to medium B with 37.5 μM cholesterol in MCD. After incubation for 90 min at 37°C, the cells were washed with PBS and switched to medium B for 2 hours at 37°C. The cells were then washed with PBS and lysed in buffer B. Samples were applied to Bolt 4 to 12% gradient gels. After electrophoresis, the proteins were transferred to nitrocellulose filters and then incubated with either anti-Flag (1:3000 dilution; Medical & Biological Laboratories Co., M185-3L) or Antibody-302 (5 μg/ml; against rat SREBP-2, department stock) at 4°C for overnight. Bound antibodies were visualized by chemiluminescence (SuperSignal West Pico Chemiluminescent Substrate, Thermo Fisher Scientific, Waltham, MA) after 1 hour of incubation with either horse anti-mouse immunoglobulin G (IgG; 1: 5000; Cell Signaling, 7076) or goat anti-rabbit IgG (1:5000; Cell Signaling, 7074) conjugated to horseradish peroxidase. The immunoblot using the horseradish peroxidase–conjugated β-actin antibody was visualized without a secondary antibody. The images were scanned using an Odyssey FC Imager (Dual-Mode Imaging System) and analyzed using Image Studio ver. 5.0 (LI-COR Biosciences, Lincoln, NE).

SUPPLEMENTARY MATERIALS

Supplementary material for this article is available at http://advances.sciencemag.org/cgi/content/full/7/34/eabh3997/DC1

View/request a protocol for this paper from *Bio-protocol*.

REFERENCES AND NOTES

1. J. L. Betters, L. Yu, NPC1L1 and cholesterol transport. *FEBS Lett.* **584**, 2740–2747 (2010).
2. S. W. Altmann, H. R. Davis Jr., L. J. Zhu, X. Yao, L. M. Hoos, G. Tetzloff, S. P. Iyer, M. Maguire, A. Golovko, M. Zeng, L. Wang, N. Murgolo, M. P. Graziano, Niemann-Pick C1 Like 1 protein is critical for intestinal cholesterol absorption. *Science* **303**, 1201–1204 (2004).
3. L. Jia, J. L. Betters, L. Yu, Niemann-Pick C1-like 1 (NPC1L1) protein in intestinal and hepatic cholesterol transport. *Annu. Rev. Physiol.* **73**, 239–259 (2011).
4. K. E. Berge, H. Tian, G. A. Graf, L. Yu, N. V. Grishin, J. Schultz, P. Kwiterovich, B. Shan, R. Barnes, H. H. Hobbs, Accumulation of dietary cholesterol in sitosterolemia caused by mutations in adjacent ABC transporters. *Science* **290**, 1771–1775 (2000).
5. L. Yu, R. E. Hammer, J. Li-Hawkins, K. von Bergmann, D. Lutjohann, J. C. Cohen, H. H. Hobbs, Disruption of Abcg5 and Abcg8 in mice reveals their crucial role in biliary cholesterol secretion. *Proc. Natl. Acad. Sci. U.S.A.* **99**, 16237–16242 (2002).
6. R. E. Temel, W. Tang, Y. Ma, L. L. Rudel, M. C. Willingham, Y. A. Ioannou, J. P. Davies, L. M. Nilsson, L. Yu, Hepatic Niemann-Pick C1-like 1 regulates biliary cholesterol concentration and is a target of ezetimibe. *J. Clin. Invest.* **117**, 1968–1978 (2007).
7. M. W. Huff, R. L. Pollex, R. A. Hegele, NPC1L1: Evolution from pharmacological target to physiological sterol transporter. *Arterioscler. Thromb. Vasc. Biol.* **26**, 2433–2438 (2006).
8. K. Narushima, T. Takada, Y. Yamanashi, H. Suzuki, Niemann-pick C1-like 1 mediates alpha-tocopherol transport. *Mol. Pharmacol.* **74**, 42–49 (2008).
9. T. Takada, Y. Yamanashi, K. Konishi, T. Yamamoto, Y. Toyoda, Y. Masuo, H. Yamamoto, H. Suzuki, NPC1L1 is a key regulator of intestinal vitamin K absorption and a modulator of warfarin therapy. *Sci. Transl. Med.* **7**, 275ra223 (2015).
10. S. Nashimoto, Y. Takekawa, Y. Takekuma, M. Sugawara, Y. Sato, Transport via Niemann-Pick C1 Like 1 contributes to the intestinal absorption of ubiquinone. *Drug Metab. Pharmacokinet.* **35**, 527–533 (2020).
11. E. Reboul, A. Klein, F. Bietrix, B. Gleize, C. Malezet-Desmoulins, M. Schneider, A. Margotat, L. Lagrost, X. Collet, P. Borel, Scavenger receptor class B type I (SR-BI) is involved in vitamin E transport across the enterocyte. *J. Biol. Chem.* **281**, 4739–4745 (2006).
12. A. Goncalves, M. Margier, S. Roi, X. Collet, I. Niot, P. Goupy, C. Caris-Veyrat, E. Reboul, Intestinal scavenger receptors are involved in vitamin K1 absorption. *J. Biol. Chem.* **289**, 30743–30752 (2014).
13. A. Goncalves, S. Roi, M. Nowicki, I. Niot, E. Reboul, Cluster-determinant 36 (CD36) impacts on vitamin E postprandial response. *Mol. Nutr. Food Res.* **58**, 2297–2306 (2014).
14. P. S. Li, Z. Y. Fu, Y. Y. Zhang, J. H. Zhang, C. Q. Xu, Y. T. Ma, B. L. Li, B. L. Song, The clathrin adaptor Numb regulates intestinal cholesterol absorption through dynamic interaction with NPC1L1. *Nat. Med.* **20**, 80–86 (2014).
15. J. L. Goldstein, R. A. DeBose-Boyd, M. S. Brown, Protein sensors for membrane sterols. *Cell* **124**, 35–46 (2006).
16. S. R. Pfeffer, NPC intracellular cholesterol transporter 1 (NPC1)-mediated cholesterol export from lysosomes. *J. Biol. Chem.* **294**, 1706–1709 (2019).
17. X. Qi, X. Li, Mechanistic insights into the generation and transduction of hedgehog signaling. *Trends Biochem. Sci.* **45**, 397–410 (2020).
18. X. Qi, P. Schmiege, E. Coutavas, X. Li, Two Patched molecules engage distinct sites on Hedgehog yielding a signaling-competent complex. *Science* **362**, eaas8843 (2018).
19. Y. Zhang, D. P. Bulkley, Y. Xin, K. J. Roberts, D. E. Asarnow, A. Sharma, B. R. Myers, W. Cho, Y. Cheng, P. A. Beachy, Structural basis for cholesterol transport-like activity of the hedgehog receptor patched. *Cell* **175**, 1352–1364.e14 (2018).
20. C. Qi, G. Di Minin, I. Vercellino, A. Wutz, V. M. Korkhov, Structural basis of sterol recognition by human hedgehog receptor PTCH1. *Sci. Adv.* **5**, eaaw6490 (2019).
21. T. Long, X. Qi, A. Hassan, Q. Liang, J. K. de Brabander, X. Li, Structural basis for itraconazole-mediated NPC1 inhibition. *Nat. Commun.* **11**, 152 (2020).
22. H. J. Kwon, L. Abi-Mosleh, M. L. Wang, J. Deisenhofer, J. L. Goldstein, M. S. Brown, R. E. Infante, Structure of N-terminal domain of NPC1 reveals distinct subdomains for binding and transfer of cholesterol. *Cell* **137**, 1213–1224 (2009).
23. X. Li, P. Saha, J. Li, G. Blobel, S. R. Pfeffer, Clues to the mechanism of cholesterol transfer from the structure of NPC1 middle lumenal domain bound to NPC2. *Proc. Natl. Acad. Sci. U.S.A.* **113**, 10079–10084 (2016).

24. M. B. L. Winkler, R. T. Kidmose, M. Szomek, K. Thaysen, S. Rawson, S. P. Muench, D. Wüstner, B. P. Pedersen, Structural insight into eukaryotic sterol transport through Niemann-Pick type C proteins. *Cell* **179**, 485–497.e18 (2019).
25. P. Saha, J. L. Shumate, J. G. Caldwell, N. Elghobashi-Meinhardt, A. Lu, L. Zhang, N. E. Olsson, J. E. Elias, S. R. Pfeffer, Inter-domain dynamics drive cholesterol transport by NPC1 and NPC1L1 proteins. *eLife* **9**, e57089 (2020).
26. H. Qian, X. Wu, X. Du, X. Yao, X. Zhao, J. Lee, H. Yang, N. Yan, Structural basis of low-pH-dependent lysosomal cholesterol egress by NPC1 and NPC2. *Cell* **182**, 98–111.e18 (2020).
27. J. H. Zhang, L. Ge, W. Qi, L. Zhang, H. H. Miao, B. L. Li, M. Yang, B. L. Song, The N-terminal domain of NPC1L1 protein binds cholesterol and plays essential roles in cholesterol uptake. *J. Biol. Chem.* **286**, 25088–25097 (2011).
28. L. Ge, J. Wang, W. Qi, H. H. Miao, J. Cao, Y. X. Qu, B. L. Li, B. L. Song, The cholesterol absorption inhibitor ezetimibe acts by blocking the sterol-induced internalization of NPC1L1. *Cell Metab.* **7**, 508–519 (2008).
29. N. H. Petersen, N. J. Faergeman, L. Yu, D. Wustner, Kinetic imaging of NPC1L1 and sterol trafficking between plasma membrane and recycling endosomes in hepatoma cells. *J. Lipid Res.* **49**, 2023–2037 (2008).
30. T. A. Johnson, S. R. Pfeffer, Ezetimibe-sensitive cholesterol uptake by NPC1L1 protein does not require endocytosis. *Mol. Biol. Cell* **27**, 1845–1852 (2016).
31. C.-S. Huang, X. Yu, P. Fordstrom, K. Choi, B. C. Chung, S.-H. Roh, W. Chiu, M. Zhou, X. Min, Z. Wang, Cryo-EM structures of NPC1L1 reveal mechanisms of cholesterol transport and ezetimibe inhibition. *Sci. Adv.* **6**, eabb1989 (2020).
32. W. Yin, E. Carballo-Jane, D. G. McLaren, V. H. Mendoza, K. Gagen, N. S. Geoghagen, L. A. McNamara, J. N. Gorski, G. J. Eiermann, A. Petrov, M. Wolff, X. Tong, L. C. Wilsie, T. E. Akiyama, J. Chen, A. Thankappan, J. Xue, X. Ping, G. Andrews, L. A. Wickham, C. L. Gai, T. Trinh, A. A. Kulick, M. J. Donnelly, G. O. Voronin, R. Rosa, A. M. Cumiskey, K. Bekkari, L. J. Mitnaul, O. Puig, F. Chen, R. Raubertas, P. H. Wong, B. C. Hansen, K. S. Koblan, T. P. Roddy, B. K. Hubbard, A. M. Strack, Plasma lipid profiling across species for the identification of optimal animal models of human dyslipidemia. *J. Lipid Res.* **53**, 51–65 (2012).
33. X. Qi, P. Schmiege, E. Coutavas, J. Wang, X. Li, Structures of human Patched and its complex with native palmitoylated sonic hedgehog. *Nature* **560**, 128–132 (2018).
34. X. Gong, H. Qian, P. Cao, X. Zhao, Q. Zhou, J. Lei, N. Yan, Structural basis for the recognition of Sonic Hedgehog by human Patched1. *Science* **361**, eaas8935 (2018).
35. X. Li, J. Wang, E. Coutavas, H. Shi, Q. Hao, G. Blobel, Structure of human Niemann-Pick C1 protein. *Proc. Natl. Acad. Sci. U.S.A.* **113**, 8212–8217 (2016).
36. H. Chen, Y. Liu, X. Li, Structure of human Dispatched-1 provides insights into Hedgehog ligand biogenesis. *Life Sci. Alliance* **3**, e202000776 (2020).
37. F. Cannac, C. Qi, J. Falschlunger, G. Hausmann, K. Basler, V. M. Korkhov, Cryo-EM structure of the Hedgehog release protein Dispatched. *Sci. Adv.* **6**, eaay7928 (2020).
38. A. Yamaguchi, R. Nakashima, K. Sakurai, Structural basis of RND-type multidrug exporters. *Front. Microbiol.* **6**, 327 (2015).
39. N. Kumar, C. C. Su, T. H. Chou, A. Radhakrishnan, J. A. Delmar, K. R. Rajashankar, E. W. Yu, Crystal structures of the *Burkholderia multivorans* hopanoid transporter HpnN. *Proc. Natl. Acad. Sci. U.S.A.* **114**, 6557–6562 (2017).
40. E. Reboul, Z. Soayfane, A. Goncalves, M. Cantiello, R. Bott, M. Nauze, F. Tercé, X. Collet, C. Coméra, Respective contributions of intestinal Niemann-Pick C1-like 1 and scavenger receptor class B type I to cholesterol and tocopherol uptake: In vivo v. in vitro studies. *Br. J. Nutr.* **107**, 1296–1304 (2012).
41. M. R. McFarlane, G. Liang, L. J. Engelking, Insig proteins mediate feedback inhibition of cholesterol synthesis in the intestine. *J. Biol. Chem.* **289**, 2148–2156 (2014).
42. M. S. Brown, A. Radhakrishnan, J. L. Goldstein, Retrospective on cholesterol homeostasis: The central role of scap. *Annu. Rev. Biochem.* **87**, 783–807 (2018).
43. A. Pirillo, A. L. Catapano, G. D. Norata, Niemann-Pick C1-like 1 (NPC1L1) inhibition and cardiovascular diseases. *Curr. Med. Chem.* **23**, 983–999 (2016).
44. Y. Y. Zhang, Z. Y. Fu, J. Wei, W. Qi, G. Baituola, J. Luo, Y. J. Meng, S. Y. Guo, H. Yin, S. Y. Jiang, Y. F. Li, H. H. Miao, Y. Liu, Y. Wang, B. L. Li, Y. T. Ma, B. L. Song, A *LIMA1* variant promotes low plasma LDL cholesterol and decreases intestinal cholesterol absorption. *Science* **360**, 1087–1092 (2018).
45. X. Li, P. Mooney, S. Zheng, C. R. Booth, M. B. Braunfeld, S. Gubbens, D. A. Agard, Y. Cheng, Electron counting and beam-induced motion correction enable near-atomic-resolution single-particle cryo-EM. *Nat. Methods* **10**, 584–590 (2013).
46. A. Rohou, N. Grigorieff, CTFFIND4: Fast and accurate defocus estimation from electron micrographs. *J. Struct. Biol.* **192**, 216–221 (2015).
47. J. Zivanov, T. Nakane, B. O. Forsberg, D. Kimanius, W. J. H. Hagen, E. Lindahl, S. H. W. Scheres, New tools for automated high-resolution cryo-EM structure determination in RELION-3. *eLife* **7**, e42166 (2018).
48. A. Punjani, J. L. Rubinstein, D. J. Fleet, M. A. Brubaker, cryoSPARC: Algorithms for rapid unsupervised cryo-EM structure determination. *Nat. Methods* **14**, 290–296 (2017).
49. P. Emsley, K. Cowtan, *Coot*: Model-building tools for molecular graphics. *Acta Crystallogr. D Biol. Crystallogr.* **60**, 2126–2132 (2004).
50. P. D. Adams, P. V. Afonine, G. Bunkóczi, V. B. Chen, I. W. Davis, N. Echols, J. J. Headd, L.-W. Hung, G. J. Kapral, R. W. Grosse-Kunstleve, A. J. McCoy, N. W. Moriarty, R. Oeffner, R. J. Read, D. C. Richardson, J. S. Richardson, T. C. Terwilliger, P. H. Zwart, PHENIX: A comprehensive Python-based system for macromolecular structure solution. *Acta Crystallogr. D Biol. Crystallogr.* **66**, 213–221 (2010).
51. G. N. Murshudov, A. A. Vagin, E. J. Dodson, Refinement of macromolecular structures by the maximum-likelihood method. *Acta Crystallogr. D Biol. Crystallogr.* **53**, 240–255 (1997).
52. V. B. Chen, W. B. Arendall III, J. J. Headd, D. A. Keedy, R. M. Immormino, G. J. Kapral, L. W. Murray, J. S. Richardson, D. C. Richardson, MolProbity: All-atom structure validation for macromolecular crystallography. *Acta Crystallogr. D Biol. Crystallogr.* **66**, 12–21 (2010).
53. A. Kucukelbir, F. J. Sigworth, H. D. Tagare, Quantifying the local resolution of cryo-EM density maps. *Nat. Methods* **11**, 63–65 (2014).
54. E. F. Pettersen, T. D. Goddard, C. C. Huang, G. S. Couch, D. M. Greenblatt, E. C. Meng, T. E. Ferrin, UCSF Chimera—A visualization system for exploratory research and analysis. *J. Comput. Chem.* **25**, 1605–1612 (2004).

Acknowledgments: The data were collected at the UT Southwestern Medical Center Cryo-EM Facility (funded in part by the CPRIT Core Facility Support Award RP170644). We thank our colleague D. Stoddard for assistance in data collection and M. Brown, J. Goldstein, and R. DeBose-Boyd for discussing and E. Debler for editing manuscript. **Funding:** This work was supported by NIH grants P01 HL020948, R01 GM134700, and R01 GM135343 and the Endowed Scholars Program in Medical Science of the UT Southwestern Medical Center and Welch Foundation (I-1957) (to X.L.). X.L. is a Damon Runyon-Rachleff Innovator supported by the Damon Runyon Cancer Research Foundation (DRR-53S-19) and a Rita C. and William P. Clements Jr. Scholar at the UT Southwestern Medical Center. **Author contributions:** T.L. purified the protein and carried out cryo-EM work. Y.L. performed the biochemical study with T.L. and Y.Q. T.L., Y.L., R.A.D.-B., and X.L. analyzed the data, and all the authors contributed to manuscript preparation. X.L. conceived the project and wrote the manuscript. **Competing interests:** The authors declare that they have no competing interests. **Data and materials availability:** The 3D cryo-EM density maps have been deposited in the Electron Microscopy Data Bank under the accession numbers EMD-24178, EMD-24179, and EMD-24180. Atomic coordinates for the atomic model have been deposited in the PDB under the accession numbers 7N4U, 7N4V, and 7N4X. All data needed to evaluate the conclusions in the paper are present in the paper and/or the Supplementary Materials.

Submitted 5 March 2021
Accepted 28 June 2021
Published 18 August 2021
10.1126/sciadv.abh3997

Citation: T. Long, Y. Liu, Y. Qin, R. A. DeBose-Boyd, X. Li, Structures of dimeric human NPC1L1 provide insight into mechanisms for cholesterol absorption. *Sci. Adv.* **7**, eabh3997 (2021).